Deformation analysis of amorphous metals based on atomic elastic stiffness coefficients

Yashiro, Kisaragi

Nishimura, K

Tomita, Yoshihiro

(Citation)
Modelling and Simulation in Materials Science and Engineering,14(4):597-605

(Issue Date)
2006-06

(Resource Type)
journal article

(Version)
Accepted Manuscript

(URL)
https://hdl.handle.net/20.500.14094/90000011

Deformation analysis of amorphous metals based on atomic elastic stiffness coefficients

K Yashiro[1], M Nishimura[2] and Y Tomita[1]

[1] Kobe University, 1-1, Rokkodai, Nada, Kobe 657-8501, JAPAN

[2] Student of Graduate School of Kobe University, 1-1, Rokkodai, Nada, Kobe 657-8501, JAPAN

E-mail: yashiro@mech.kobe-u.ac.jp

Abstract. The elastic limit of a crystal can be evaluated by the positiveness of elastic stiffness coefficients, B_{ijkl}. We had demonstrated that the nucleation of lattice defects such as a dislocation and cleavage cracking can be predicted by the atomic B_{ijkl} at each atom point. The amorphous metals and bulk metallic glasses draw intense interest whether the criteria is applicable or not since they are regarded as " ultimate " of lattice defects. In the present study, an amorphous Ni-Al binary alloy is made by a usual melt-quench simulation and subjected to tension by means of molecular dynamics simulation. During the simulations, the positiveness of atomic B_{ijkl} is discussed for all atoms. Contrary to a Ni-Al crystal, many atoms show negative value even in the initial equilibrium of the amorphous before loading. These "unstable" atoms turn out to be the non-clustered atom or the outer-shell of the local cluster such as 12(0,0,12,0) icosahedron. On the other hand, the center atoms of the local clusters show high stability resulting in the positive B_{ijkl} of the whole system. It is also demonstrated that the change in the atomic B_{ijkl} can reveal the collapse and re-configuration of local clusters during the deformation.

1. Introduction

Amorphous metals are widely used as magnetic head or anticorrosion plating materials, utilizing the superior corrosion resistance, magnetic and mechanical properties. So far they are fabricated as film or ribbon due to the ultra rapid cooling rate; however, Inoue et al. found that some alloys don't crystallize from the supercooled liquid metal even in the very low cooling rate, and newly categorized into "bulk metallic glasses" [1]. In the last decade enormous efforts have been made to seek a new bulk metallic glass with larger and larger bulk shape [1]. The bulk metallic glasses are anticipated to be new structural materials in the use of characteristic properties of amorphous structure. However, the deformation theory of metals, *e.g.* the crystal plasticity or the dislocation theories, cannot be applied to amorphous metals since they have no crystal structure nor slip planes. Thus many studies have been involved to reveal the inherent characteristic of amorphous structure and model the deformation and fracture of amorphous metals.

In the present study, an amorphous metal is made by usual melt-quench simulation and subjected to tension by means of molecular dynamics as the past studies; however, the deformation and stability of local clusters are discussed from a unique viewpoint of the "local lattice stability". The lattice stability analysis [2, 3] has been originally proposed to evaluate the ideal strength of infinite homogeneous lattices (continuum). The deformation of an idealized crystal can be represented with a few variables describing the Bravais lattice, so that the second order derivatives, or Hessian, of the energy function can be strictly derived to assess the stability. Wang et al. [4, 5] have proposed the stability criteria based on the positiveness of the elastic stiffness coefficients, B_{ijkl}, to involve the effect of internal inhomogeneity such as thermal vibration. Then we have extended the stability criteria to evaluate the local deformation such as nucleation of lattice defects, *e.g.* dislocation or cleavage crack, by using the atomic elastic stiffness coefficients, B^{α}_{ijkl} [6]. In the atomic simulations, the B^{α}_{ijkl} is determined by the surrounding atom configuration within the cutoff radius, so that we can calculate the local stability at each atom point even in the amorphous structure without any lattice. Amorphous metals or bulk metallic glasses draw intense interest whether the criteria is applicable or not since they are regarded as "ultimate" of lattice defects.

2. Interatomic potential and atomic elastic stiffness coefficients

The interaction of atoms are represented with the embedded atom method (EAM) [7, 8] potential. In the EAM formulation the total energy, E_{tot}, is evaluated by

$$E_{\mathrm{tot}} = \frac{1}{2}\sum_{\alpha}\sum_{\beta(\neq\alpha)}\phi_{t_\alpha t_\beta}(r^{\alpha\beta}) + \sum_{\alpha}F_{t_\alpha}(\overline{\rho}^{\alpha}) \tag{1}$$

with

$$\overline{\rho}^{\alpha} = \sum_{\beta(\neq\alpha)}\rho_{t_\beta}(r^{\alpha\beta}) \tag{2}$$

where $r^{\alpha\beta}$ is the scalar distance between atom α and atom β, ϕ is the pairwise interaction between atoms, $\overline{\rho}^{\alpha}$ is the "density" at atom α given by the superposition of the another pairwise interaction, $\rho(r)$, from neighboring atoms, and $F(\overline{\rho})$ is the "embedding function". t_α and t_β are the type of atom α and β, respectively, and the functions ϕ, $\rho(r)$, $F(\overline{\rho})$ depend on atom types. The functions and parameters of $\rho(r)$ and $\phi(r)$ for Ni and Al binary system are described in the original papers proposed by Voter et al. [9, 10]. The details of the potential functions are described in our previous paper of dislocations in Ni-based superalloys [11].

In the thermodynamics theory of crystal lattices [12], the stress, σ_{ij}, and the elastic coefficients, C_{ijkl}, at current state (whichever the crystal is deformed or not) are defined as the first and second order derivatives of the internal energy, U. That is,

$$\sigma_{ij} = \frac{1}{V}\left(\frac{\partial U}{\partial \eta_{ij}}\right) \tag{3}$$

$$C_{ijkl} = \frac{1}{V}\left(\frac{\partial^2 U}{\partial\eta_{ij}\partial\eta_{kl}}\right), \tag{4}$$

where η_{ij} is the virtual infinitesimal strain and V the volume of crystal at the state. Hereafter all indices obeys the summation convention. The elastic stiffness coefficient, B_{ijkl}, which relates the stress with the actual strain, ε_{ij}, is written as

$$B_{ijkl} \equiv \left(\frac{\partial\sigma_{ij}}{\partial\varepsilon_{kl}}\right) = C_{ijkl} + \frac{1}{2}(\sigma_{il}\delta_{jk} + \sigma_{jl}\delta_{ik} + \sigma_{ik}\delta_{jl} + \sigma_{jk}\delta_{il} - 2\sigma_{ij}\delta_{kl}) \tag{5}$$

where δ_{ij} is Kronecker's delta.

Eq.(1) is regarded as the sum of following contribution of each atom,

$$E^\alpha = \frac{1}{2}\sum_{\beta(\neq\alpha)} \phi_{t_\alpha t_\beta}(r^{\alpha\beta}) + F_{t_\alpha}(\overline{\rho}^\alpha), \tag{6}$$

so that we can formulate the atomic stress, σ_{ij}^α, and the atomic elastic coefficients, C_{ijkl}^α, by differentiating Eq.(6) regarding to virtual infinitesimal strain as follows;

$$\sigma_{ij}^\alpha = \frac{1}{\Omega}\sum_{\beta(\neq\alpha)}\left\{\frac{1}{2}\phi'_{\alpha\beta} + F'_\alpha\rho'_{\alpha\beta}\right\}\frac{r_i^{\alpha\beta}r_j^{\alpha\beta}}{r^{\alpha\beta}} \tag{7}$$

$$\begin{aligned} C_{ijkl}^\alpha = \frac{1}{\Omega}\Bigg[&\sum_{\beta(\neq\alpha)}\left\{\frac{1}{2}\left(\phi''_{\alpha\beta} - \frac{\phi'_{\alpha\beta}}{r^{\alpha\beta}}\right) + F'_\alpha\left(\rho''_{\alpha\beta} - \frac{\rho'_{\alpha\beta}}{r^{\alpha\beta}}\right)\right\}\frac{r_i^{\alpha\beta}r_j^{\alpha\beta}r_k^{\alpha\beta}r_l^{\alpha\beta}}{(r^{\alpha\beta})^2} \\ &+ F''_\alpha\left\{\sum_{\beta(\neq\alpha)}\rho'_{\alpha\beta}\frac{r_i^{\alpha\beta}r_j^{\alpha\beta}}{r^{\alpha\beta}}\right\}\left\{\sum_{\gamma(\neq\alpha)}\rho'_{\alpha\gamma}\frac{r_k^{\alpha\gamma}r_l^{\alpha\gamma}}{r^{\alpha\gamma}}\right\}\Bigg] \end{aligned} \tag{8}$$

where Ω is the atomic volume, F_α, $\rho_{\alpha\beta}$ and $\phi_{\alpha\beta}$ denote $F_{t_\alpha}(\bar{\rho}^\alpha)$, $\rho_{t_\beta}(r^{\alpha\beta})$ and $\phi_{t_\alpha t_\beta}(r^{\alpha\beta})$, respectively, and the prime means the derivative of each function.

In the isothermal process, we should consider *not* the internal energy, U, *but* the Helmholtz free energy, F [12]. By considering the partition function of the canonical ensemble, stress fluctuation term emerges in the second order derivative of the Helmholtz free energy (Ray's fluctuation formula) [13, 14]. That is, the stress fluctuation soften the elastic coefficients, if we calculate them during a long time period under the equilibrium at elavated temperature. However, the fluctuation formula can be applied only for whole the system under the static equilibrium, while our focus is on the dynamic and local process under ongoing deformation. Thus we have adopted the formulation above mentioned. In our previous simulation, the largest fluctuation term is calculated as much as 5% of the second order derivative of the potential energy (Born term) at the temperature of 300 K.

3. Simulation procedure

Ni and Al atoms are randomly located on the fcc lattice point in a cubic cell of $10.63\text{nm}\times10.63\text{nm}\times10.63\text{nm}$ ($30\times30\times30$ fcc unit lattices). The total number of atoms

is 108 000 and the composition of Ni and Al is set to 3:1. This initial structure is relaxed during 15 000 MD step at the temperature of $T = 300\,\mathrm{K}$ as a "crystal". The periodic boundary conditions are applied in all directions. The time increment of MD calculation is 1 fs and the temperature is controlled by velocity scaling. Then the crystal is melt during 10 000 fs MD calculation at $T = 3\,000\,\mathrm{K}$. The temperature is rapidly quenched to 300 K with the cooling rate of $-2 \times 10^{13}\,\mathrm{K/s}$. The "amorphous" is derived by additional relaxation of 15 000 MD step at $T = 300\,\mathrm{K}$. During the simulations, the normal stress is kept at zero by expanding/compressing the cell size.

Both the crystal and amorphous is then subjected to tension by elongating the cubic cell. A small strain increment is applied on the cell at every MD step, resulting in the strain rate of 1×10^9 /s. The loading axis is [001] in the case of the crystal. The atom position is normalized by the cell length so that the distance of each atom is uniformly expanded in the loading process. The cell length in the transverse directions is also controlled to cancel the normal stress originated by the Poisson's contraction. The temperature is kept at 300 K during the tension.

4. Results and discussions

4.1. Sructure of melt-quenched configuration

Figure 1(a) shows the radial distribution functions of liquid metal at $T = 3\,000\,\mathrm{K}$ and the equilibrium state after the melt-quench simulation. The second peak in the function of melt-quenched metal clearly shows the dissociation into two sub-peaks. Figure 1(b) illustrates the distribution of typical Voronoi polyhedra in the crystal, liquid metal and melt-quenched structure. The percentage of Voronoi polyhedrons are shown according to the number of Voronoi planes, f, and its index, $(\mathrm{n}_3, \mathrm{n}_4, \mathrm{n}_5, \mathrm{n}_6)$, which indicates the number of triangle, tetragonum, pentagon and hexagon in the Voronoi planes, respectively. It is obvious that the melt-quenched structure is different from the liquid metal. In particular, the icosahedron of 12(0,0,12,0), which has no translational symmetry so that doesn't appear in the crystal, remarkably increases after the melt-quench simulation. These facts deduce that the equilibrium structure is in the amorphous state.

4.2. Stress–strain curves and atom migration

Figure 2(a) indicates the relationships between the stress and strain of the crystal and amorphous under tension. The crystal shows the linear increase up to the strain about 0.1 with the peak stress of about 11 GPa. Then the stress suddenly drops by the nucleation of many partial dislocations as carefully reported in our previous study [6]. On the other hand, the amorphous shows nonlinear curve from the very beginning of the loading. After a small peak stress of 3 GPa around the strain of 0.06, the stress slightly decreases and the amorphous deforms without stress increase. Figure 2(b) illustrates the magnitude and direction of migration of each atoms with small vectors. The atom

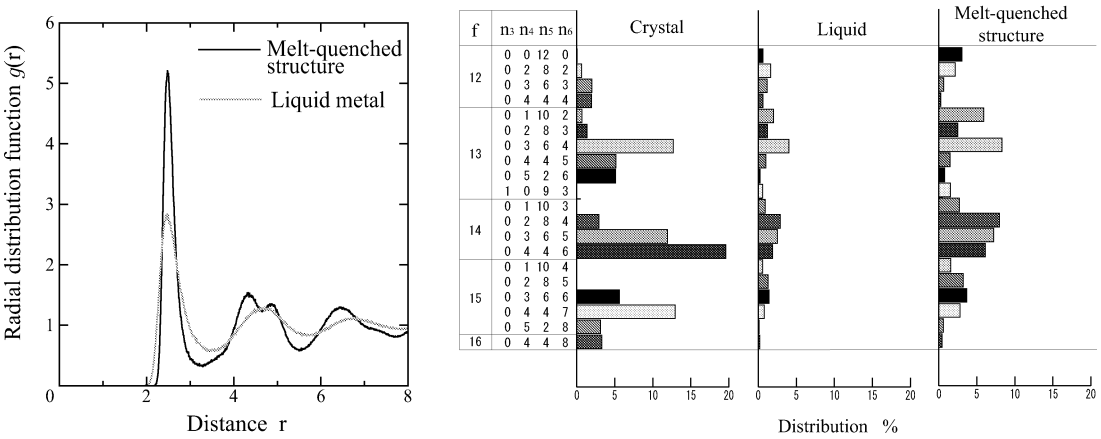

(a) Radial distribution function (b) Distribution of typical Voronoi polyhedra

Figure 1. Structure analysis before and after melt-quench simulation.

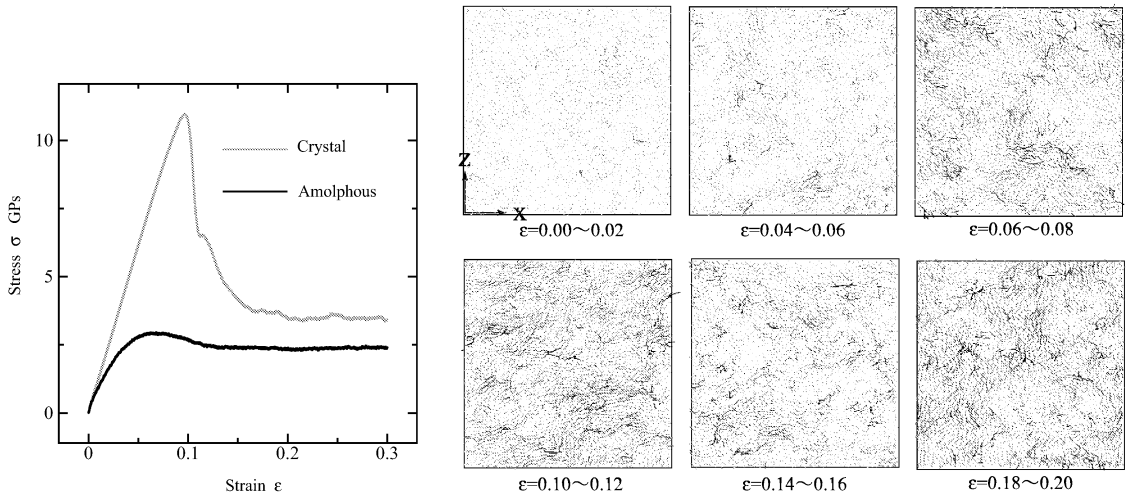

(a) Stress–strain curves. (b) Atom migration in the amorphous under tension.

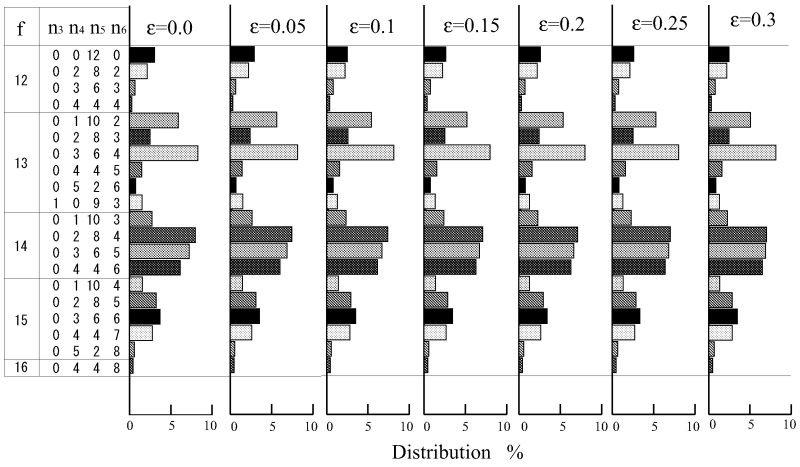

(c) Change in Voronoi polyhedra.

Figure 2. Deformation behavior of amorphous metal under tension.

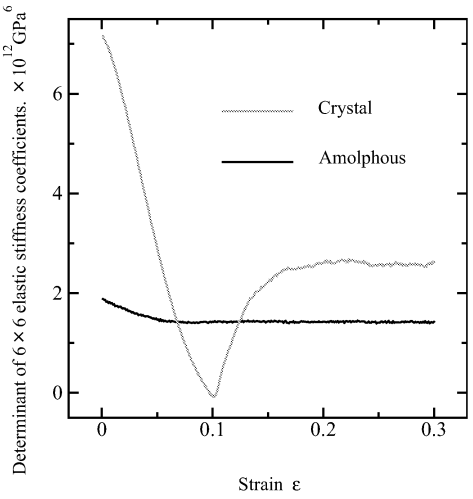

Figure 3. Change in the system stability of crystal and amorphous under tension.

migration is normalized by the cell length and evaluated at each interval of $\Delta\varepsilon = 0.02$. Moreover, only a thin part of the cell is drawn to avoid scrawl of many arrows in three-dimensional space. The atom migration is rather small before the peak strain of $\varepsilon = 0.06$, while it shows large and collective motion after the peak. The local deformation takes place here and there and draws vortex like trajectories. The atom motion can be identified as "stringlike cooperative motion" and has been intensely investigated on the basis of critical distance for interstitials [15, 16, 17]. It should be noted that the periodic boundary condition prevents the nucleation of global shear deformation, *e.g.* shear band, in the present simulation; however, it doesn't affect the local deformation since there is a sufficient degree of freedom in the simulation cell as confirmed from the fact that many dislocations appear in the simulation of crystal. Figure 2(c) shows the change in the percentage of Voronoi polyhedra during the tension; however, we cannot find any marked change. The radial distribution function also maintains the same shape as in Fig.1(a) during the tension, although it is not shown. From these facts we can deduce that the amorphous maitains its structure despite the local configuration changes by the inhomogeneous deformation as shown in Fig.2(b).

4.3. Change in the stability of crystal and amorphous under tension

Figure 3 shows the change in the magnitude of the determinant of B_{ijkl} of the whole crystal/amorphous, or the Wang's stability criteria [4, 5]. Here the determinant is for the 6×6 matrix of B_{IJ}, which is Voigt notation [12] of the symmetric part of B_{ijkl}, since they dominates the stability [4, 5]. The determinant of the crystal is far larger than that of amorphous at $\varepsilon = 0$. Then it drastically decreases and become negative at the peak strain of 0.1, resulting in the nucleation of many dislocations. The system stability of crystal recovers by the relaxation with dislocations and shows constant magnitude in the later stage of $\varepsilon > 0.15$. This drastic change has great importance

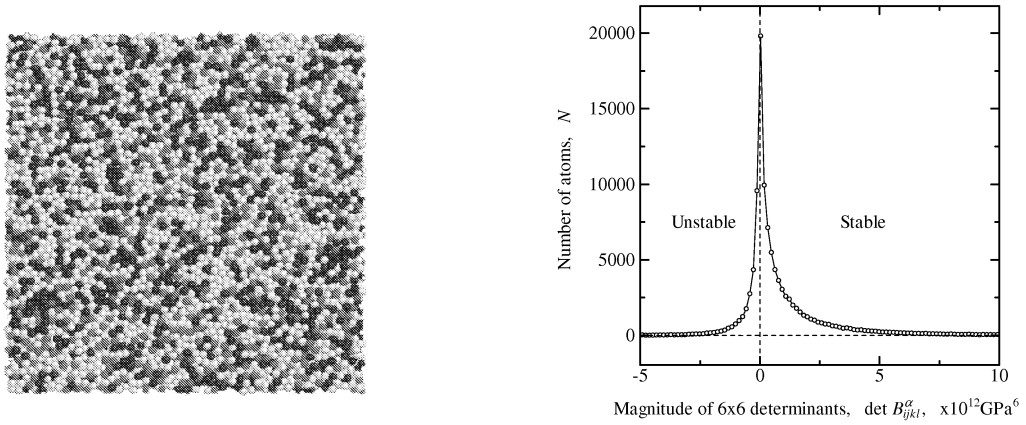

(a) Unstable atoms of $\det B^{\alpha}_{ijkl} < 0$.

(b) Distribution in $\det B^{\alpha}_{ijkl}$.

Figure 4. Distribution of unstable atoms and the magnitude of $\det B^{\alpha}_{ijkl}$ at $\varepsilon = 0$.

since it implies the transition from the homogeneous deformation of a perfect crystal to the inhomogeneous one with many lattice defects. The stability of amorphous is smaller than that of deformed crystal even in the initial equilibrium at $\varepsilon = 0$; however, it shows positive value or the structure is "stable". The stability decreases as the strain increase, however, it never becomes negative since the inhomogeneous deformation takes place from the onset of the loading. The stability reaches bottom at the strain of $\varepsilon = 0.06$, where the stress–strain curve shows the peak. After the strain the amorphous deforms with constant stability as in the case of crystal with many defects. The difference in the later stage of $\varepsilon > 0.2$ might signify the different characteristics between amorphous and crystal with defects. It is of great interest to clarify whether the stability of polycrystal approaches that of amorphous or not when the grain size is reduced smaller and smaller. We have already performed such simulations and revealed that the stability of nanocrystal ultimately converges to that of amorphous and sometimes becomes slightly lower depending on the density; however, the details cannot be discussed here for lack of space.

4.4. Local stability in amorphous structure

Figure 4(a) shows the snapshot of atoms in the amorphous at $\varepsilon = 0$. The bright and middle shaded spheres are stable Ni and Al atoms, respectively, while the black ones are the "unstable" atoms of $\det B^{\alpha}_{ijkl} < 0$. The crystal have few unstable atoms in the initial equilibrium. The amorphous is considered as the "ultimate" of defects so that it is natural that there are many unstable atoms even in the equilibrium state. The amorphous, however, is judged as "stable" from the system elastic stiffness of B_{ijkl}, which is identical to the average of atomic stiffness B^{α}_{ijkl}, as above mentioned. That is, the amorphous should have atoms which show high stability to compensate the amorphous structure. Figure 4(b) indicates the distribution in $\det B^{\alpha}_{ijkl}$ at $\varepsilon = 0$. It

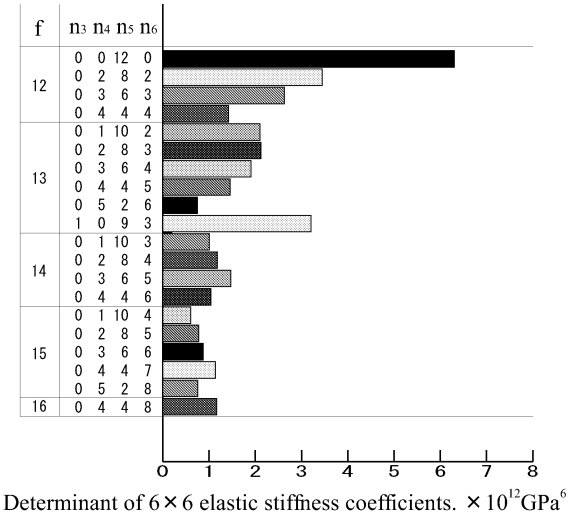

Figure 5. Distribution of det B^{α}_{ijkl} of the center atoms of typical Voronoi polyhedra.

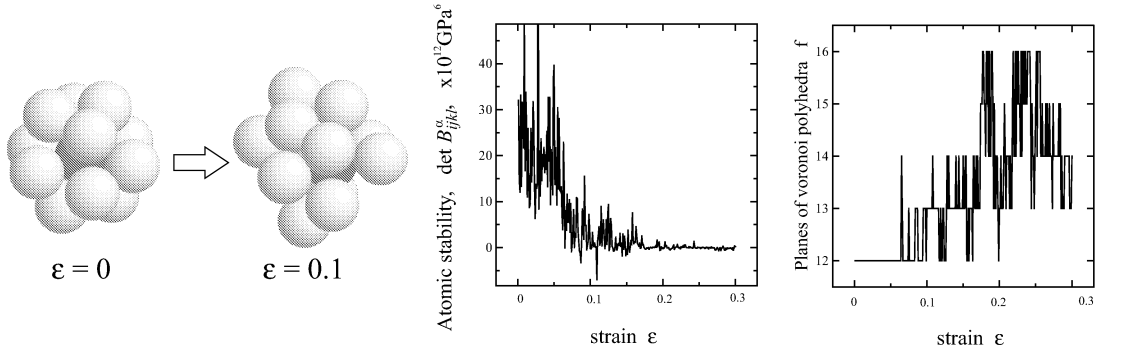

(a) Collapse of local icosahedron

(b) Change in the atomic stability of center atom of the collapsed cluster

(c) Change in planes of Voronoi polyhedra

Figure 6. Collapse of an icosahedron and its change in det B^{α}_{ijkl} and Voronoi planes.

has an intense peak at det $B^{\alpha}_{ijkl} = 0$. In the liquid state under elavated temperature, all atoms shows nearly zero of det B^{α}_{ijkl} and symmetric distribution with respect to det $B^{\alpha}_{ijkl} = 0$. On the other hand, the amorphous shows wider distribution on the stable side, thus the system stiffness of det B_{ijkl} becomes positive. Figure 5 shows the magnitude of det B^{α}_{ijkl} of the center atoms of typical Voronoi clusters. The 12(0,0,12,0) icosahedron shows the highest stability, and we can find that the local clusters of 12(0,2,8,2) and 13(1,0,9,3), which are close family of 12(0,0,12,0), have higher stability than the others. Thus the system stability is increased by the short-range order clusters typical in the amorphous structure.

Figure 6 shows the snapshot of a local cluster, and the change in det B^{α}_{ijkl} and Voronoi planes of its center atom. The cluster is judged as icosahedron at $\varepsilon = 0$, however, collapses during tension as shown in Fig. 6(a). It is noteworthy that the strain where the det B^{α}_{ijkl} becomes zero coincides with the point where the number of Voronoi planes

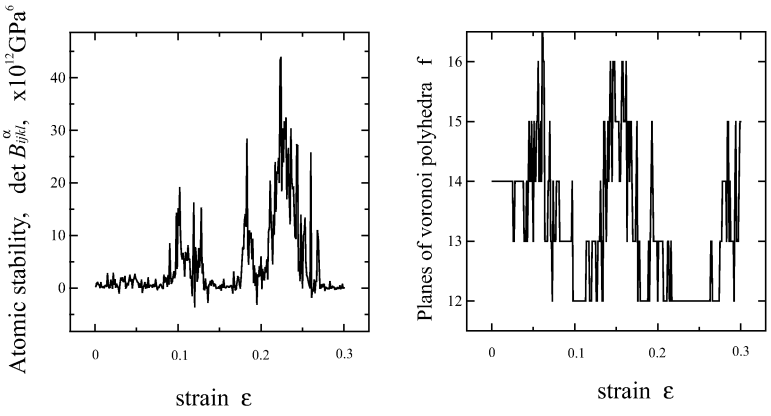

(a) Change in the atomic stability (b) Change in planes of Voronoi polyhedra

Figure 7. Change in det B^{α}_{ijkl} and Voronoi planes of an atom.

change. The local cluster actually collapses at the strain as already shown in Fig. 6(a). Figure 7 shows the change in det B^{α}_{ijkl} and Voronoi planes of another atom. The atom does not make icosahedron at $\varepsilon = 0$, however, it forms icosahedron temporarily around $\varepsilon = 0.10, 0.17$ and $0.20 \sim 0.26$ as can be seen in Voronoi planes. The change in det B^{α}_{ijkl} definitely exhibits such cluster formation, collapse and reconstruction. The Voronoi analysis has rather ambiguity in the definition of local cluster from surrounding atoms, so that the number of planes shows flip-flop change. The atomic stability is judged only with the positiveness of atomic elastic stiffness coefficients and doesn't have such ambiguity. Thus the collapse and re-construction of local clusters are easily clarified by tracing the atomic stability.

5. Conclusion

In the present study, an amorphous metal is made by usual melt-quench simulation and subjected to tension by means of molecular dynamics as the past studies; however, the deformation and stability of local clusters are discussed from a unique viewpoint of the positiveness of atomic elastic stiffness coefficients, B^{α}_{ijkl}. The determinant of the elastic stiffness for the whole amorphous, B_{ijkl}, which is the average of B^{α}_{ijkl}, decreases to its minimum at the peak strain under the tension; however, it never becomes negative while that of a perfect crystal does at the peak strain and recovers by the nucleation and glide of dislocations. This difference is attributed to the local inhomogeneous deformation in the amorphous structure. On the positiveness of det B^{α}_{ijkl} of each atom, the amorphous have many "unstable" atoms even in the equilibrium before tension. These unstable atoms turn to be non-cluster or outer-shell atoms of local clusters. The determinant of B^{α}_{ijkl} definitely denotes the highest stability of icosahedron in the amorphous structure. It is also suggested that the collapse and re-construction of local clusters are easily clarified by tracing the positiveness of B^{α}_{ijkl}.

References

[1] Inoue A 2000, *Acta Mater.*, 48, 279.
[2] Born M and Huang K 1954, *Dynamical Theory of Crystal Lattices*, Oxford UP.
[3] Milstein F 1971, *Phys. Rev.* B, **3**, 1130.
[4] Wang J, Yip S, Phillpot S R and Wolf D 1993, *Phys. Rev. Lett.*, **71**, 4182.
[5] Wang J, Li J, Yip S Phillpot S R and Wolf D 1995, *Phys. Rev.* B, **52**, 12627.
[6] Yashiro K and Tomita Y 2001, *Journal de Physique* IV, **11**, Pr5–3.
[7] Daw M S and Baskes M I 1983, *Phys. Rev. Lett.*, **50**, 1285.
[8] Daw M S and Baskes M I 1984, *Phys. Rev.* B, **29**, 6443.
[9] Voter A F and Chen S P 1987, *Mat. Res. Soc. Symp. Proc.*, **82**, 175.
[10] Voter A F 1994, *Intermetallic Compounds: Vol.1, Principles*, 77, John Wiley & Sons.
[11] Yashiro K, Naito M and Tomita Y 2001, *Int. J. Mech. Sci.*, **44**, 1845.
[12] Wallace D C 1972, *Thermodynamics of Crystals*, Wiley, Newyork.
[13] Ray J R and Garben H W 1981, *Molecular Physics*, **43**, 1293.
[14] Ray J R 1982, *Journal of Applied Physics*, **53**, 6441.
[15] Granato A V 1992, *Phys. Rev. Lett.*, **68**, 974.
[16] Kob W, Donati C, Plimpton S J, Poole P H and Glotzer S C 1997, *Phys. Rev. Lett.*, **79**, 2827.
[17] Nordlund K, Ashkenazy Y, Averback R S and Granato A V 2005, *Europhys. Lett.* **71**, 625.